JACC: CLINICAL ELECTROPHYSIOLOGY VOL. 3, NO. 7, 2017

ISSN 2405-500X
http://dx.doi.org/10.1016/j.jacep.2016.11.010

NEW RESEARCH PAPERS

Massive Accumulation of Myofibroblasts in the Critical Isthmus Is Associated With Ventricular Tachycardia Inducibility in Post-Infarct Swine Heart

Tarvinder S. Dhanjal, PhD,[a,b] Nicolas Lellouche, MD,[b] Christopher J. von Ruhland, PhD,[a] Guillaume Abehsira, MD,[b] David H. Edwards, PhD,[a,c] Jean-Luc Dubois-Randé, MD, PhD,[b] Konstantinos Moschonas, MB BCh,[a] Emmanuel Teiger, MD,[b] Alan J. Williams, PhD,[a,c] Christopher H. George, PhD[a,c]

JACC: CLINICAL ELECTROPHYSIOLOGY CME/MOC

This article has been selected as the month's *JACC: Clinical Electrophysiology* CME/MOC activity, available online at www.jacc-electrophysiology.org by selecting the *JACC* Journals CME/MOC tab.

Accreditation and Designation Statement

The American College of Cardiology Foundation (ACCF) is accredited by the Accreditation Council for Continuing Medical Education (ACCME) to provide continuing medical education for physicians.

The ACCF designates this Journal-based CME/MOC activity for a maximum of 1 *AMA PRA Category 1 Credit(s)*. Physicians should only claim credit commensurate with the extent of their participation in the activity.

Method of Participation and Receipt of CME/MOC Certificate

To obtain credit for *JACC: Clinical Electrophysiology* CME/MOC, you must:

1. Be an ACC member or *JACC: Clinical Electrophysiology* subscriber.
2. Carefully read the CME/MOC-designated article available online and in this issue of the journal.
3. Answer the post-test questions. At least 2 out of the 3 questions provided must be answered correctly to obtain CME/MOC credit.
4. Complete a brief evaluation.
5. Claim your CME/MOC credit and receive your certificate electronically by following the instructions given at the conclusion of the activity.

CME/MOC Objective for This Article: Upon completion of this activity, the learner should be able to understand the cellular substrate at the border zone of scar related ventricular tachycardia and possible ties to ventricular tachycardia susceptibility in a post-infarct swine model.

CME/MOC Editor Disclosure: CME/MOC Editor Smit Vasaiwala, MD, has nothing to declare.

Author Disclosures: This study was funded by the British Heart Foundation, Association pour la Recherche et l'Etude des Maladies CARdiovasculaires (AREMCAR), Cardiac Research & Development Fund, and Cardiff University. The authors have reported that they have no relationships relevant to the contents of this paper to disclose.

Medium of Participation: Print (article only); online (article and quiz).

CME/MOC Term of Approval

Issue Date: July 2017
Expiration Date: June 30, 2018

From the [a]School of Medicine, Cardiff University, Cardiff, Wales, United Kingdom; [b]Hôpital Henri Mondor Albert Chenevier, DHU-ATVB, Inserm U955, IMRB, University Paris Est Creteil Paris XII, Paris, France; and the [c]Institute of Life Sciences, Swansea University Medical School, Swansea, Wales, United Kingdom. This study was funded by the British Heart Foundation, Association pour la Recherche et l'Etude des Maladies CARdiovasculaires (AREMCAR), Cardiac Research & Development Fund, and Cardiff University. The authors have reported that they have no relationships relevant to the contents of this paper to disclose.

Manuscript received October 24, 2016; accepted November 17, 2016.

JACC: CLINICAL ELECTROPHYSIOLOGY VOL. 3, NO. 7, 2017
JULY 2017:703–14

Massive Accumulation of Myofibroblasts in the Critical Isthmus Is Associated With Ventricular Tachycardia Inducibility in Post-Infarct Swine Heart

Tarvinder S. Dhanjal, PhD,[a,b] Nicolas Lellouche, MD,[b] Christopher J. von Ruhland, PhD,[a] Guillaume Abehsira, MD,[b] David H. Edwards, PhD,[a,c] Jean-Luc Dubois-Randé, MD, PhD,[b] Konstantinos Moschonas, MB BCh,[a] Emmanuel Teiger, MD,[b] Alan J. Williams, PhD,[a,c] Christopher H. George, PhD[a,c]

ABSTRACT

OBJECTIVES In this study the authors determined the extent of cellular infiltration and dispersion, and regional vascularization in electrophysiologically (EP) defined zones in post-myocardial infarction (MI) swine ventricle.

BACKGROUND The critical isthmus (CI) in post-MI re-entrant ventricular tachycardia (VT) is a target for catheter ablation. In vitro evidence suggests that myofibroblasts (MFB) within the scar border zone (BZ) may increase the susceptibility to slow conduction and VT, but whether this occurs in vivo remains unproven.

METHODS Six weeks after mid-left anterior descending coronary artery occlusion, EP catheter-based mapping was used to assess susceptibility to VT induction. EP data were correlated with detailed cellular profiling of ventricular zones using immunohistochemistry and spatial distribution analysis of cardiomyocytes, fibroblasts, MFB, and vascularization.

RESULTS In pigs with induced sustained monomorphic VT (mean cycle length: 353 ± 89 ms; n = 6) the area of scar that consisted of the BZ (i.e., between the normal and the low-voltage area identified by substrate mapping) was greater in VT-inducible hearts (iVT) than in noninducible hearts (non-VT) ($p < 0.05$). Scar in iVT hearts was characterized by MFB accumulation in the CI (>100 times that in normal myocardium and >5 times higher than that in the BZ in non-VT hearts) and by a 1.7-fold increase in blood vessel density within the dense scar region extending towards the CI. Sites of local abnormal ventricular activity potentials exhibited cellularity and vascularization that were intermediate to the CI in iVT and BZ in non-VT hearts.

CONCLUSIONS The authors reported the first cellular analysis of the VT CI following an EP-based zonal analysis of iVT and non-VT hearts in pigs post-MI. The data suggested that VT susceptibility was defined by a remarkable number of MFB in the VT CI, which appeared to bridge the few remaining dispersed clusters of cardiomyocytes. These findings define the cellular substrate for the proarrhythmic slow conduction pathway. (J Am Coll Cardiol EP 2017;3:703–14)

Scar-related re-entry is the most common cause of sustained monomorphic ventricular tachycardia (VT) in patients post-myocardial infarction, which is primarily due to fibrosis-mediated slow conduction and conduction block (1,2). The electrical and structural remodeling post-MI is complex, and in humans, dynamic infarct remodeling several years after the acute event leads to the formation of re-entrant VT circuits. Specifically, scar-related VT re-entry possesses a critical isthmus (CI) or conducting channel that localizes to the VT exit site and is composed of a small mass of undefined tissue (2–9). This region is the primary target for catheter ablation, and previous human and large animal studies using 3-dimensional electroanatomic and magnetic resonance imaging (MRI)-based mapping techniques have defined the VT CI within heterogeneous border zone (BZ) areas as "areas of viable myocardium interwoven with scar" (7–10). However, although altered electrical activity and dysfunctional resistivity in the CI has been suggested (1,11), there is an absence of cellular characterization of the CI within the BZ to explain the observed slow conduction within this region.

The contributions of stromal cells, which include cardiac fibroblasts (FB) and myofibroblasts (MFB), to myocardial dysfunction have been considered, and it has been established that the behavior of MFB within the heart is different compared with the healing process in other organs, and may be a pathological determinant of heart disease (12,13). Post-MI, endogenous FB are activated to differentiate into MFB, which converge on the damaged region and accelerate the synthesis of various extracellular matrix (ECM) proteins critical for scar development (14–16). In response to humoral and mechanical cues (e.g., transforming growth factor-beta, angiotensin II, endothelin-1, micro-RNAs, such as miR-21 (17), and altered mechanical tension [18]), MFB persist chronically in healed human infarcts. This is distinct from the transient existence of MFB in other fibrotic tissues (e.g., liver and skin), which suggests that MFB play a role in maintaining the structural and functional integrity of infarct territory long after the acute injury has resolved.

SEE PAGE 715

Although there is compelling in vitro and computational modeling evidence to suggest that the increased numbers and/or regional heterogeneity of MFB in the post-MI myocardium increases the susceptibility to slow conduction and VT in humans (12,14,15,17,19), the presence of MFB within the CI component of the re-entrant VT circuitry in vivo remains unproven (20). To specifically address this issue we: 1) investigated the composition, extent and spatial distribution of cellular infiltrates in electrophysiologically (EP)-defined ventricular zones in a swine model of post-MI re-entrant VT; 2) quantified the extent of vascularization in these regions; and 3) reconciled these data with the propensity for VT induction.

METHODS

LEFT ANTERIOR DESCENDING CORONARY ARTERY OCCLUSION AND MI INDUCTION IN PIGS. We used a validated pig model of mid-left anterior descending (LAD) balloon occlusion to recapitulate clinically relevant features of human myocardium post-MI, including: 1) transmural ST-segment elevation MI with comparable electrocardiographic (ECG) changes observed in humans post-MI; 2) a similar ratio of scar size-to-myocardial area, which is a critical determinant of post-MI VT susceptibility; 3) human-like coronary vasculature with low collateral flow and the rare occurrence of surface intercoronary anastomosis; and 4) MRI-based and 3-dimensional electroanatomic mapping evidence that post-infarct re-entrant VT circuits are comparable to the ventricular arrhythmias that develop in MI survivors (7,21–24).

Coronary artery occlusion in healthy adult female domestic pigs (*S. scrofa domesticus*; 40 to 60 kg) was performed using an angioplasty balloon as described in the Online Appendix. All studies were performed in accordance with European Union Directive 2010/63/EU, the position of the American Heart Association on Research Animal Use (1984), and the ARRIVE (Animal Research Reporting in Vivo Experiments) guidelines on the reporting animal experiments (25). All protocols were approved by the local institutional Animal Care and Use Committee of the Centre Hospitalier Universitaire Henri Mondor (INSERM: U955).

EP MAPPING OF VT. Six weeks after coronary artery occlusion, MI pigs were subjected to a detailed left ventricular substrate map during sinus rhythm using an electroanatomic mapping system (CARTO XP, Biosense Webster, Diamond Bar, California) (Online Appendix). The bipolar voltage parameters to correlate histologically determined scar within the pig chronic infarct model were previously described (21,26).

Programmed electrical stimulation was used to assess VT inducibility using a validated pig protocol (27) (Online Appendix). The endpoint of testing was either completion of the protocol to refractoriness or consistent induction of sustained monomorphic VT, which was defined as lasting 15 s, and confirmed on the surface 12-lead ECG (7–9). If sustained monomorphic VT was successfully induced, pace mapping was performed to locate VT isthmus sites, defined as pace mapping sites where the QRS morphology matched ≥11 of 12 leads on the ECG, with the VT having paced latencies >40 ms (7–9,28) (Online Figure 1).

Ventricular zones 1 to 4 were categorized on the basis of the following EP characteristics:

- Zone 1: dense scar (voltage area bipolar <1 mV);
- Zone 2: BZ region containing the VT CI site, which was defined as a voltage area bipolar between 1 and 2 mV, with a good pace map (≥11 of 12 lead match);
- Zone 3: BZ region with a voltage area between 1 and 2 mV, with a poor pace map (<11 of 12 lead match);
- Zone 4: adjacent normal voltage myocardium with a voltage area bipolar >2 mV (**Figure 1,** Online Figure 2).

ABBREVIATIONS AND ACRONYMS

α-SMA = α-smooth muscle actin
BZ = border zone
CI = critical isthmus
cTnT = cardiac troponin T
CM = cardiomyocytes
ECM = extracellular matrix
EP = electrophysiology
FB = fibroblasts
IHC = immunohistochemistry
iVT = inducible ventricular tachycardia
LAD = left anterior descending
LAVA = local abnormal ventricular activity
MFB = myofibroblasts
MI = myocardial infarction
MRI = magnetic resonance imaging
Vim = vimentin
VT = ventricular tachycardia
vWF = von Willebrand factor

FIGURE 1 Electroanatomic Histological Overlay

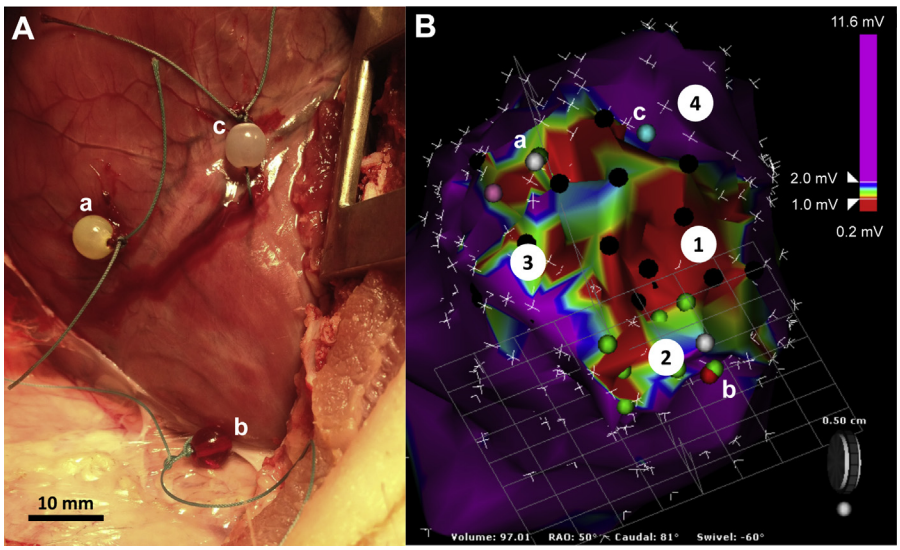

(A) Epicardial markers **(a, b, c)** were sutured at the corresponding location on the **(B)** 3-dimensional electroanatomic map to identify functionally distinct electrophysiologically defined zones (see Methods). **Purple dots**, late and/or local abnormal ventricular activity; **black and green dots**, poor and good pace maps with <11 of 12 and ≥11 of 12 electrocardiographic leads matching the ventricular tachycardia, respectively.

By definition, zone 2 is absent in those hearts in which VT cannot be induced.

In addition to substrate mapping, pace mapping, and entrainment mapping to locate the VT CI site, location markers were assigned to late potentials and complex local abnormal ventricular activity (LAVA) potentials (29).

To correlate 3-dimensional substrate maps with histological assessments of left ventricular sections without recourse to endocardial ablation lesions, a mini-thoracotomy was performed, and location markers were sutured at the corresponding epicardial surface at 3 locations using the mapping catheter (Figure 1). At the conclusion of the EP study, the animals were killed using a fatal administration of propofol, and the heart was immediately explanted. Left ventricular specimens were immediately fixed in 4% (v/v) neutral buffered formaldehyde (300 ml) in preparation for histological analysis.

TABLE 1 Characterization of Post-MI Myocardium in Inducible and Noninducible VT Hearts

	Inducible VT (n = 6)	Noninducible VT (n = 6)	p Value
CARTO points	393 ± 50	454 ± 112	0.34
LV mass (g)	145 ± 14	146 ± 3	0.87
Voltage area bipolar <2 mV (cm^2)	26 ± 4	27 ± 12	0.52
Voltage area bipolar <1 mV (cm^2)	10 ± 1	16 ± 7	0.005*
Border zone area (cm^2)	17 ± 3	11 ± 5	0.055
Border zone area (% scar)	64 ± 2	41 ± 3	0.004*

Values are mean ± SE. *Significant difference between groups.
LV = left ventricular; VT = ventricular tachycardia.

TISSUE PROCESSING AND IMMUNOHISTOCHEMISTRY. Ventricular tissue was sectioned and processed for immunohistochemistry (IHC) as described in the Online Appendix. Sections were stained with antibodies against α-smooth muscle actin (α-SMA), von Willebrand factor (vWF), vimentin (Vim), and cardiac troponin-T (cTnT) (Online Appendix). MFB were defined as $\alpha\text{-SMA}^{+}/\text{vWF}^{-}$ cells and FB as $\alpha\text{-SMA}^{-}/\text{Vim}^{+}$ cells. Cardiomyocytes (CM) were identified on the basis of cTnT immunoreactivity (cTnT^{+}). Endovascular endothelial cells were defined as $\alpha\text{SMA}^{-}/\text{vWF}^{+}$ and vascular smooth muscle cells were defined as $\alpha\text{-SMA}^{+}/\text{vWF}^{+}$ cells.

QUANTIFYING THE SPATIAL DISTRIBUTION OF CELLS AND BLOOD VESSELS IN MYOCARDIAL SECTIONS. A method for calculating the spatial distribution of cells in zones 1 to 4 was developed based on "grid occupancy," in which cellular distribution is assigned values between 0 and 1; 0 describes the most spatially restricted signal (i.e., maximum clustering),

FIGURE 2 **Histological Assessments of Zones 1 to 4 in Post-Myocardial Infarction Ventricles**

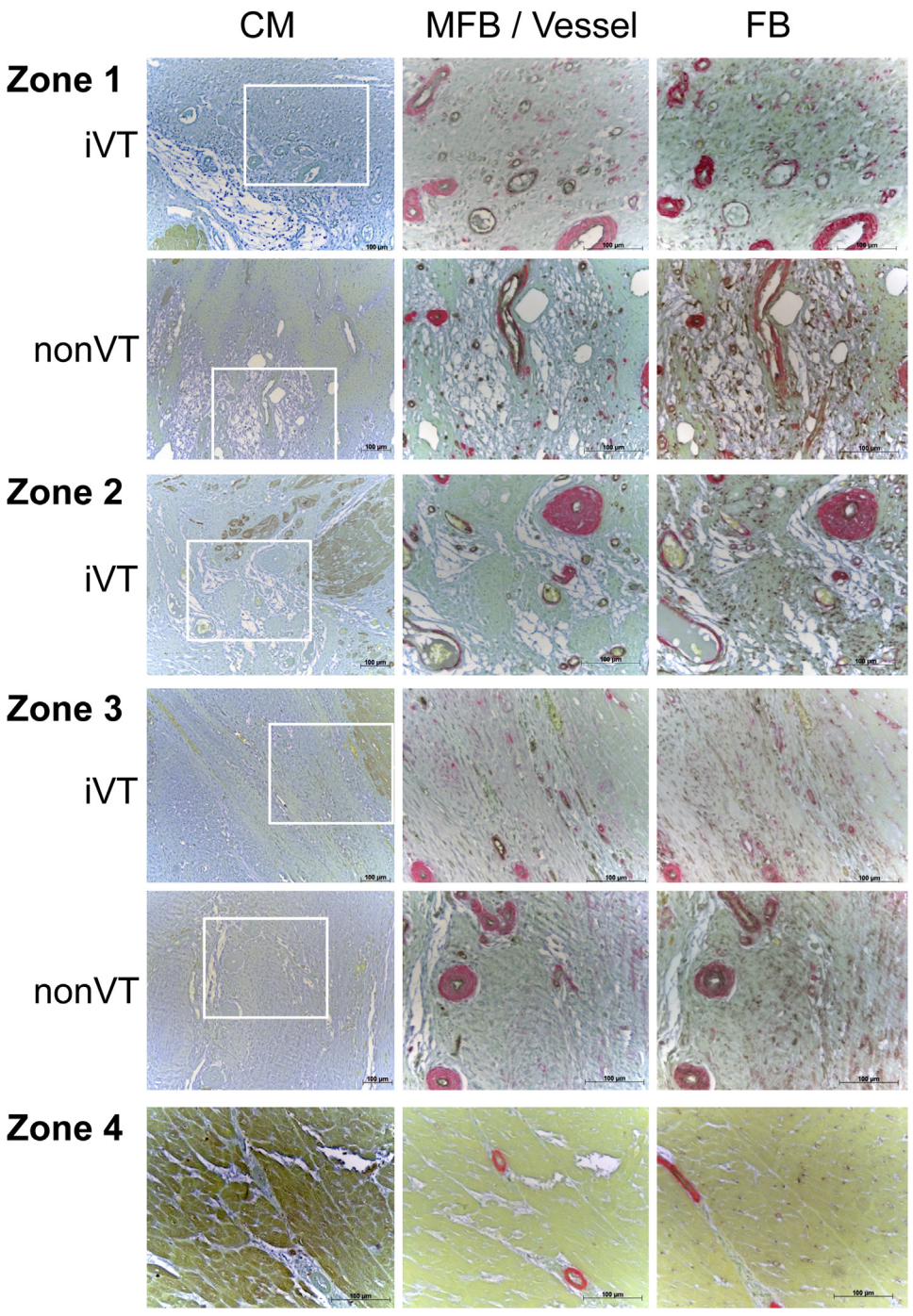

Ventricular sections were stained for cardiomyocytes (CM) (cardiac troponin T–positive) **(brown; left panels)**, myofibroblasts (MFB) (α-smooth muscle actin–positive/von Willebrand factor–negative [α-SMA^{+}/vWF^{-}) **(red),** and endothelium and/or blood vessels (α-SMA^{+}/vWF^{+}) (co-incident **red and black; middle panels**), and fibroblasts (FB) (α-SMA^{-}/vimentin-positive) **(black; right panels)**. Light green and picromethylblue were used to visualize cellularity and connective tissue and/or the extracellular matrix, respectively (Online Appendix). **Boxes outlined in white** (0.15 mm^{2}) are magnified in the **middle and right panels**. iVT = inducible ventricular tachycardia; VT = ventricular tachycardia.

FIGURE 3 Zonal Analysis of Cellularity and Vascularization in iVT and Non-VT Hearts

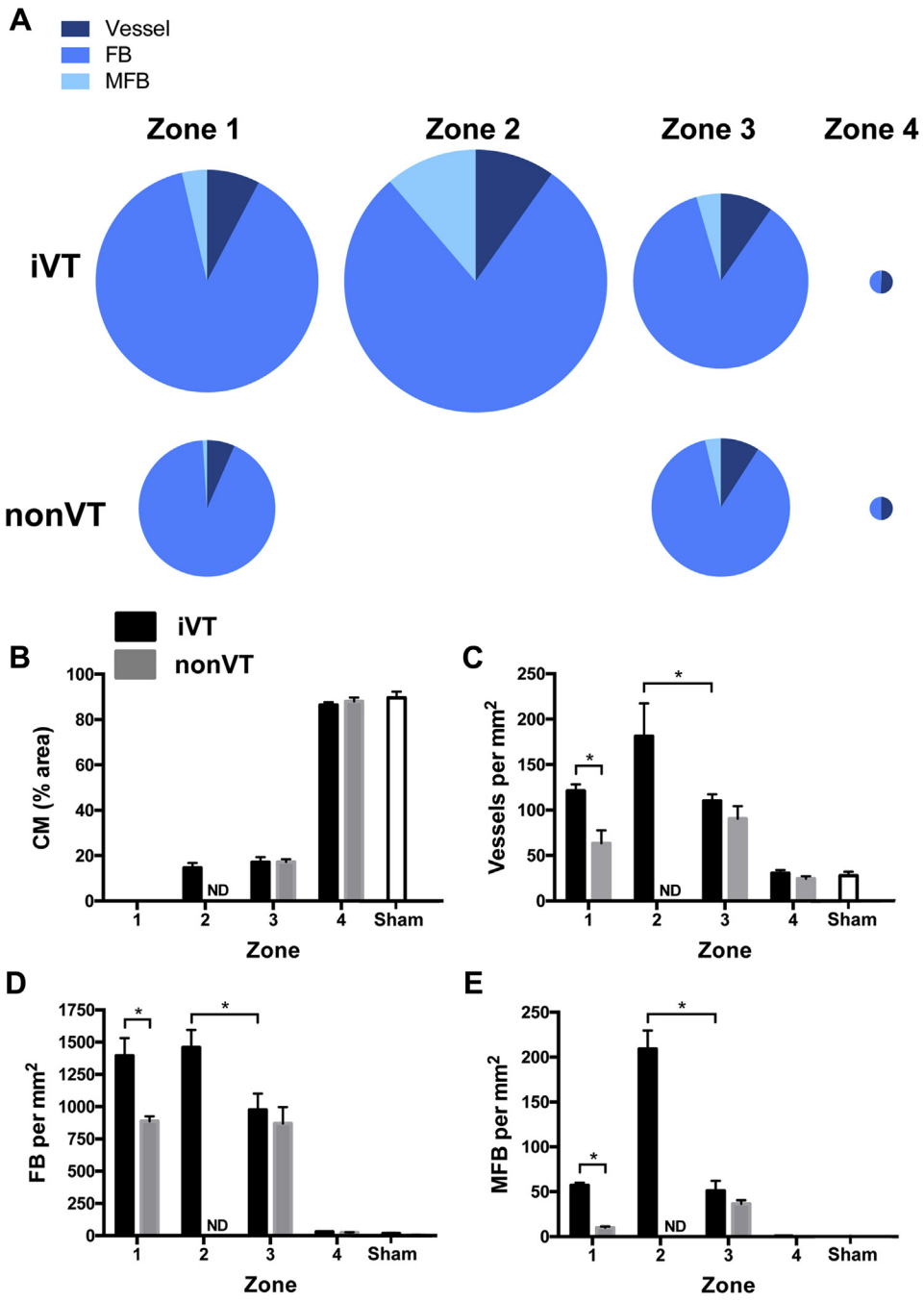

(A) The relative proportion of MFB, FB, and vessels in zones 1 to 4 in iVT and non-VT hearts. The diameter of the circle is directly proportional to the cumulative number of cells per square millimeter. Because CM were analyzed using a different method (percentage of area coverage), these data are omitted here. Quantification of **(B)** CM, **(C)** blood vessels, **(D)** FB, and **(E)** MFB in zones 1 to 4 in iVT **(black)** and non-VT **(gray)** hearts. *$p < 0.05$. Data are from 5 and 4 iVT and non-VT hearts, respectively (4 to 7 sections for each zone per heart). All parameters in zones 1 to 3 are significantly different from normal myocardium (zone 4) in iVT and non-VT hearts, and from hearts from sham-operated control pigs ($p < 0.05$). Sham data are from 2 pigs (8 to 10 sections for each zone per pig). ND = not determined due to the absence of zone 2 in non-VT hearts; other abbreviations as in Figure 2.

FIGURE 4 Cellular Distribution and MFB Alignment Does Not Correlate With VT Inducibility

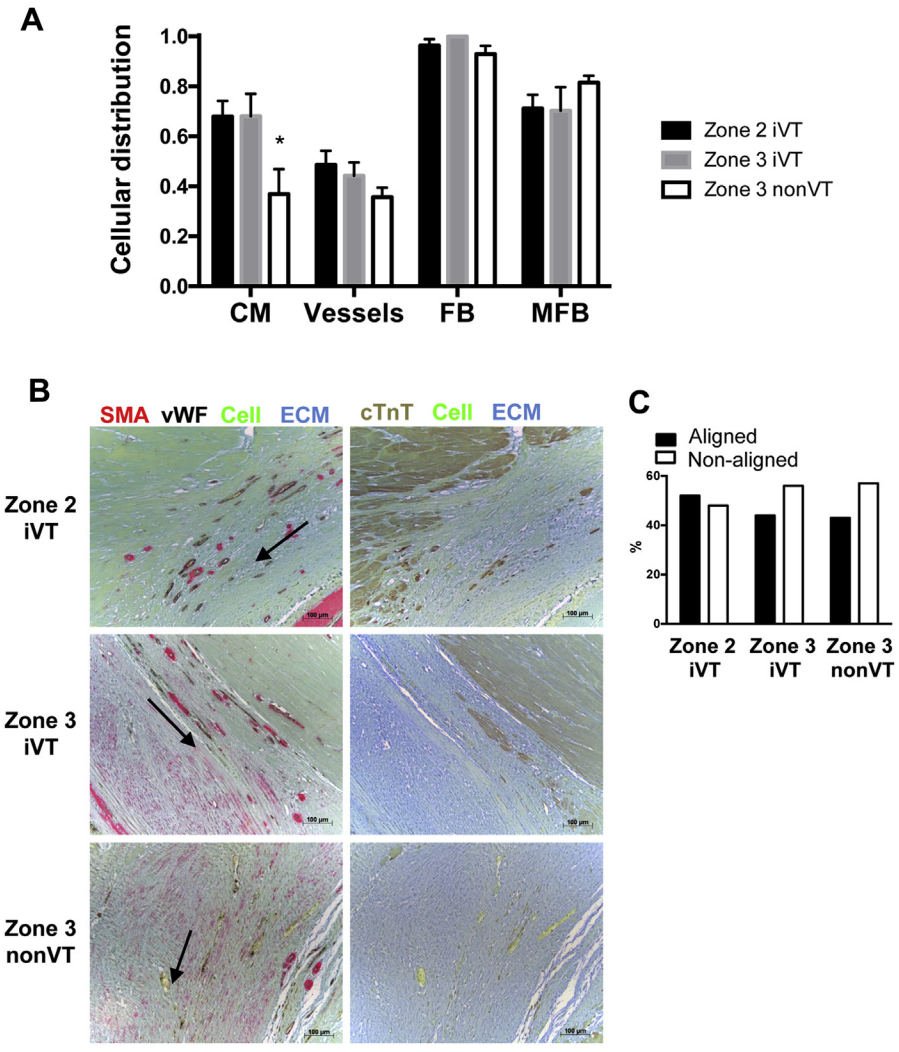

(A) The spatial distribution of CM, MFB, FB, and blood vessels in zones 2 and 3 in iVT hearts and zone 3 in non-VT hearts was calculated (Online Figure 3). iVT (n = 5) and non-VT hearts (n = 4) and data are from the following number of sections: zone 2 iVT (29), zone 3 iVT (27), and zone 3 nonVT (23). *p < 0.05. **(B)** Conduits of directionally oriented MFB **(arrow)** in representative sections of zone 2 (iVT) and zone 3 (iVT and non-VT). **(C)** Relative axial alignment of MFB. Number of experiments is given in **(A)**. ECM = extracelluar matrix; other abbreviations as in **Figure 2**.

whereas 1 denotes the maximum possible distribution of an IHC signal over a given area. This process is shown in Online Figure 3.

STATISTICAL ANALYSIS. Data were tested for normality using D'Agostino-Pearson test. Normally- and non-normally distributed data were compared using analysis of variance and/or Student's *t*-test or Kruskal-Wallis and/or Mann-Whitney tests, respectively. Contingency tables were constructed for chi-square testing of categorical variables. p values <0.05 were considered statistically significant. In linear regression analysis, a Pearson (r^2) coefficient >0.30 and p value of the slope of regression line <0.05 was accepted as an index of correlation. All statistical analysis was performed using Prism 6.0 (GraphPad Inc, La Jolla, California).

RESULTS

INCREASED BZ AREA IN VT-INDUCIBLE HEARTS. Six weeks following mid-LAD coronary artery occlusion,

FIGURE 5 Late/LAVA Potentials Exhibit Cellular Profile Intermediate Between CI and BZ Regions

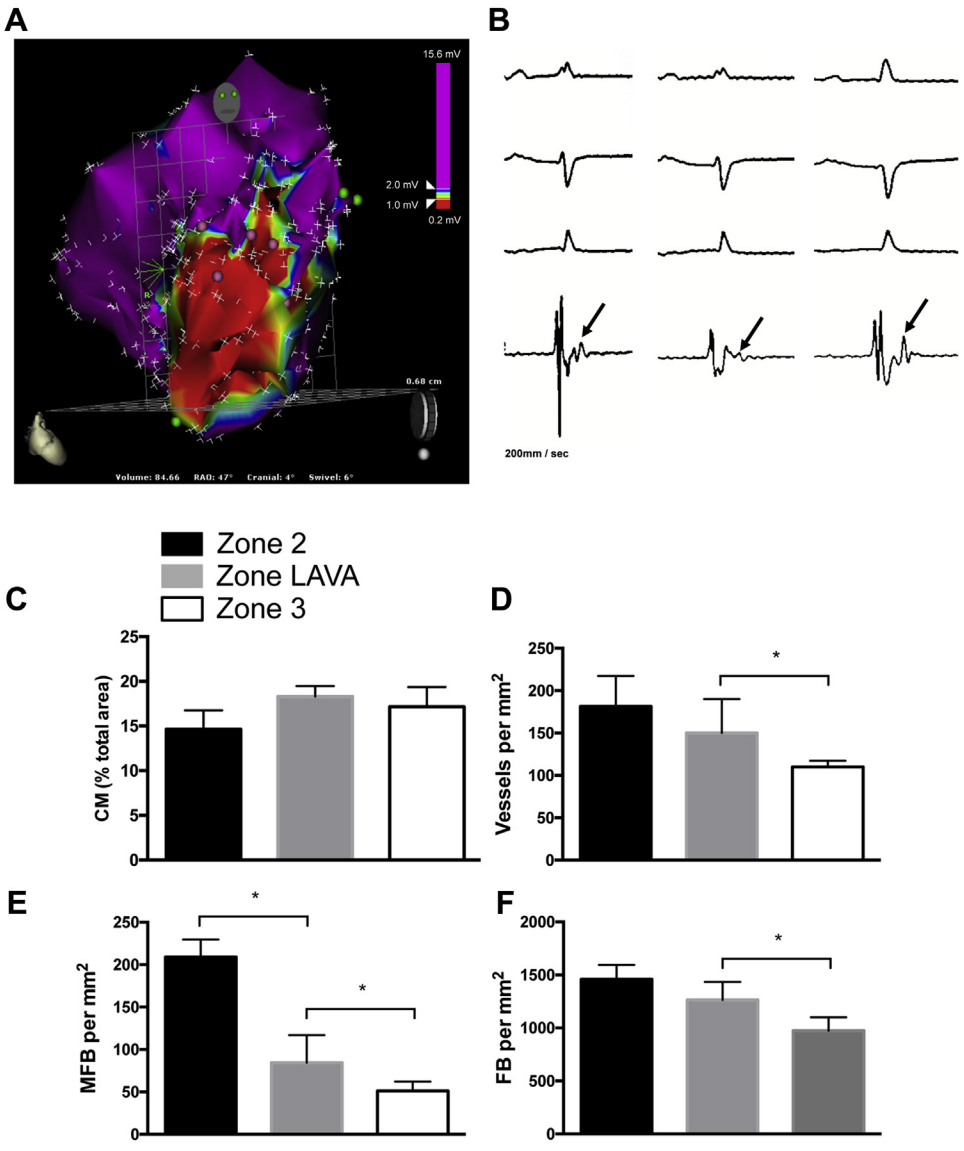

(A) Substrate map of late and/or LAVA sites **(pink dots)** located within the superior aspect of the border zone (BZ). **(B)** The corresponding surface electrocardiographic leads (I, II and III) in sinus rhythm and local bipolar electrograms at 3 of these LAVA sites **(left, middle, right panels)**. **Arrows** indicate late and/or LAVA potentials. Analysis of the abundances of **(C)** CM, **(D)** blood vessels, **(E)** MFB, and **(F)** FB in late and/or LAVA potential sites compared with zones 2 (VT critical isthmus [CI]) and 3 (BZ regions with poor pace map) in iVT hearts (data from Figure 3B to 3E). Seventeen sections obtained from 3 iVT hearts (pigs 4, 11, and 16) were analyzed. The single incidence of late and/or LAVA potentials in a non-VT heart (pig 6) was not analyzed. *$p < 0.05$. Abbreviations as Figures 1 and 2.

12 pigs underwent detailed EP assessment to probe their susceptibility to VT induction (Online Table). Sustained monomorphic VT was reproducibly induced in 6 pigs (mean VT cycle length: 353 ± 89 ms), and 6 pigs were refractory to VT induction (**Table 1 and** Online Table). Detailed substrate maps were constructed for the left ventricle with no difference in the number of sampling points in VT inducible (iVT) versus non-inducible (non-VT) hearts (**Table 1**). Scar size (i.e., zones 1 to 3) (**Figure 1**) was similar in both groups, but the area of dense scar (i.e., zone 1) was significantly greater in non-VT hearts (**Table 1**). The extent of the BZ (i.e., zones 2 and 3; mean number of sampling sites per heart: 65 ± 11) was

significantly greater in iVT hearts (Table 1). All VTs were hemodynamically unstable; therefore, pace mapping was used to identify the CI in iVT hearts at multiple sites along the BZ.

MFB ACCUMULATION DEFINES THE CI IN IVT HEARTS. IHC was performed on sections from zones 1 to 4 (Figure 1) in iVT hearts from pigs 4, 7, 9, 11, and 16, and zones 1, 3, and 4 in non-VT hearts from pigs 5, 6, 13, and 15 (Online Table, Figure 2, Online Figure 2). We did not perform IHC on pig 8 (EP mapping errors), 10 (post-occlusion ventricular fibrillations), and 14 (suboptimal fixation). Two sham-operated animals (17 and 18) were used as control animals.

There were regional differences in cellular composition in VT versus non-VT hearts. Zone 1 dense scarring in iVT hearts exhibited an increased number of regions devoid of cells versus non-VT hearts (Figure 2). Elsewhere, the overall cellularity of BZ (zones 2 and 3) and normal myocardium (zone 4) was no different between iVT and non-VT hearts, and both groups exhibited a profile similar to that of normal myocardium in sham-operated animals (Figure 2, Online Figure 4B). Likewise, the abundance and spatial distribution of ECM deposition in zones 1 to 4 in iVT and non-VT hearts was similar and was comparable to that in the normal myocardium of sham-operated pigs (Figure 2, Online Figure 4B). Noninfarcted myocardium in both iVT and non-VT hearts (zone 4) consisted almost entirely of CM. There were equivalently low numbers of blood vessel-associated endothelial cells ($<40/mm^2$) and FB ($<30/mm^2$), and negligible or no MFB (iVT hearts, <1 MFB/mm^2; non-VT hearts, zero) in both groups, which was entirely consistent with measurements that define the normal myocardium (Figures 3B to 3E). In contrast, scarred regions (zones 1 to 3) in iVT and non-VT hearts were characterized by the enrichment of vessels, FB, and MFB compared with noninfarcted myocardium (zone 4) (3.9, 42.9, and >1,000 times that of normal ventricular tissue [zone 4], respectively) ($p < 0.001$) (Figure 3A).

Zone 1 dense scar was characterized by a total loss of CM (Figure 3B), but there was a substantial enrichment in vascularization (relative enrichment of 4.2 [iVT] and 2.5 [non-VT]), FB (relative enrichment of 52 [iVT] and 36 [non-VT]), and MFB (relative enrichment 18 [iVT]) compared with the respective normal myocardium (zone 4, normalized value assigned 1). The extent of vascularization (Figure 3C), and the number of FB (Figure 3D) and MFB (Figure 3E) in zone 1 was significantly higher in iVT hearts compared with non-VT hearts (relative increase of 1.9, 1.6, and 5.7, respectively; $p < 0.05$).

Zone 3 in iVT and non-VT hearts exhibited a similar level of loss of CM (~80%) compared with adjacent noninfarcted myocardium (Figure 3B). In contrast, zone 3 in iVT and non-VT hearts was characterized by the enrichment of vessels, FB, and MFB to that determined in zone 1, and the cellular profile was not different between groups (i.e., FB >> vessel > MFB > CM) (Figures 3B to 3E). Importantly, blood vessel density and MFB infiltration was remarkably high in the VT CI (zone 2), and we determined that the relative enrichment of vessels, FB, and MFB in zone 2 compared with zone 3 in iVT hearts was 1.7, 1.5, and 5.4, respectively (Figures 3B to 3E). Except for the significant positive correlation between the densities of MFB and FB in zone 3 in iVT hearts, no other correlation between cellular abundances existed (Online Figure 5).

HOMOGENEOUS DISTRIBUTION OF MFB, FB AND VESSELS IN BZ IN iVT AND NON-VT HEARTS. To investigate whether the difference in VT inducibility was associated with the altered spatial distribution of vascularization, MFB, and FB, we developed a method for quantifying the spatial distribution of the component cells (Online Figure 3). Blood vessels, FB, and MFB were similarly distributed in BZ (zones 2 and 3) in both iVT and non-VT hearts (Figure 4A). The reduced index of CM distribution in zone 3 (i.e., increased clustering) was a defining feature of non-VT hearts (Figure 4A) and did not correlate with the distribution of vessels or MFB (Online Figure 6).

MFB in zones 2 and 3 commonly exhibited directional alignment in "conduits" that extended over several hundred micrometers ($n = 79$ sections) (Figure 4B). The incidence of conduit formation was equivalent in iVT and non-VT hearts (Figure 4C), which suggested that this phenomenon probably did not represent a causative event in increasing VT susceptibility.

LATE AND/OR LAVA POTENTIALS REPRESENT SITES OF CI EVOLUTION. It has been suggested that late and/or LAVA potentials have the potential to evolve into susceptibility foci for VT CI (29), and we extended the study to reconcile EP mapping of late and/or LAVA potentials with IHC analysis of the BZ in iVT and non-VT hearts. We identified an isolated LAVA site in only 1 non-VT heart (pig 6). In contrast, late and/or LAVA potentials were abundantly identified in 3 iVT hearts (pigs 4, 5, and 16), with a mean occurrence of 10 ± 3 sites per heart

(**Figures 5A and 5B**). CM density was similar within LAVA sites compared with the VT CI (zone 2) and in the BZ with poor pace maps (zone 3) within the iVT scar (**Figure 5C**). However, LAVA sites were characterized by a density of vascular-associated cells (**Figure 5D**), MFB (**Figure 5E**), and FB (**Figure 5F**) that was intermediate to that determined in the VT CI (zone 2) and in the BZ with poor pace maps (zone 3).

DISCUSSION

DEFINING THE CELLULAR SUBSTRATE OF VT. The cellular substrate of post-MI VT has been poorly understood, but we reported the cellular signature of the VT CI and showed that iVT scar was defined by the remarkable accumulation of stromal cells (MFB and/or FB; MFB) and an increased density of blood vessels within the dense scar region that extended toward the VT CI.

A previous study of VT in dogs post-MI mapped lines of conduction block within the VT circuit and suggested the existence of electrical coupling between heterogeneous cell types (11). The present work corroborated and extended these findings, and revealed that the exceptionally high density of MFB in the VT CI, which was 100 times greater than in noninfarcted myocardium (zone 4) and more than 5 times that determined in the BZ in non-VT hearts (zone 3), might fundamentally contribute to VT susceptibility. The concurrently enriched vascularization in the VT CI (1.7 times greater than that in the BZ of non-VT hearts) was also notable because approximately 50% of MFB within the scar might originate from bone marrow precursor cells (30). It is not yet clear whether such increased vascularization leads to the increased recruitment of MFBs or whether the higher density of MFBs releases proangiogenic factors that result in the higher vascular cell density (31).

MFB ACCUMULATION, SLOW CONDUCTION PATHWAYS, AND A LIKELY ROLE FOR HETEROCELLULAR MFB-CM COUPLING. Our data defined the VT CI as a specialized region of the BZ in which the few remaining clusters of CM are bridged via abundant MFB. De Bakker et al. (1) previously investigated the mechanism of slow conduction, a pre-requisite of VT inducibility, in post-MI human papillary muscle. A "zig zag" pattern of high-speed activation through the infarcted tissue was described, secondary to branching and merging bundles of CM ensheathed by collagenous septa (1). Although not directly demonstrated, these investigators postulated that activation delays possibly arose as a consequence of increased tissue heterogeneity and altered resistance due to heterocellular coupling (i.e., CM to non-CM interactions) (1). In support of this hypothesis, it has been suggested that the few (viable) CM that remained in the post-MI scar could couple with MFB via gap junctions (32), and that homocellular (MFB-MFB) or heterocellular (MFB-CM) coupling could plausibly induce slow conduction by partial depolarization of CM (33) and also underpin ectopic activity via depolarization-induced automaticity (21,22,26,27). Our data were entirely consistent with a model of heterocellular connectivity in which increased MFB density in the VT CI could promote MFB-MFB and MFB-CM connectivity, or alternatively, that the increased clustering of CM in the BZ of non-VT hearts (**Figure 4A**) might protect against the slow conduction required for re-entrant VT (32,33). Although these findings contributed to a collective weight of evidence that heterocellular coupling contributes to arrhythmogenesis by adversely modulating the directionality and speed of electrical coupling within this region and with adjacent regions of the myocardium (11,31), currently, there is no direct evidence to corroborate the existence of such coupling in vivo. Further work is necessary to unequivocally resolve these issues.

The quantification of FB and MFB populations post-MI also raised intriguing issues regarding the dynamic transition of cell phenotype and differentiation within the scar region. We showed that late and/or LAVA potentials, the elimination of which was reported to improve VT ablation outcome (29), were associated with a cellular profile intermediate between the VT CI (zone 2) and BZ sites (zone 3). This finding supported the idea that LAVA sites might evolve into CI sites, but further work is required to definitively determine whether their early ablation is of clinical benefit.

STUDY LIMITATIONS. We acknowledge some limitations of the present investigations.

The method used to detect VT exit sites involved the conduction of the activation wavefront from a site of origin that lies within a region of scar to the endocardial surface via conduction through preferential fibers. When pacing is performed, capture of the myocardium surrounding the catheter tip might result in a QRS complex that reflects local capture that is different from the native QRS complex of the VT.

The hemodynamic instability of all VTs limited our ability to perform entrainment maneuvers, and thus, not all VTs might have been macro-re-entrant in

nature. Others reported micro-re-entrant VT from a focal source in pig models of post-MI VT (23,24).

Although we studied numerous sections corresponding to the component zones (135 sections in total), the sampling of each section consisted of 5 randomly selected areas each of 0.6 mm^2 (Online Figure 2). Therefore, our analysis represented a limited assessment of the total area of the post-MI scar.

MFB and FB populations were distinguished on the basis of α-SMA^+/vWF^- and α-SMA^-/Vim^+ immunotyping, respectively; at present, no better alternatives are available. Assigning discrete molecular signatures to these cell populations—and also potentially phenotypically different subpopulations—will be important.

Quiescent cardiac FB activate spontaneously and differentiate into MFB in vitro, although the extent to which these observations accurately reflect the properties of FB to MFB transition in cardiac tissue in vivo remains controversial (34). Therefore, because transdifferentiation of FB into MFB will likely lead to different FB/MFB ratios, our conclusions are based on the chosen time point of the study (i.e., 6 weeks post-MI).

Consistent with the notion that the 6-week scar is "living," we did not observe the massive ECM deposition characteristic of later scarring, which suggested that the pathogenic laying down of ECM takes >6 weeks in this model. It will be important to determine the implications of the present data for patients who present at longer follow-up post-MI (e.g., 2 to 10 years).

CONCLUSIONS

These data defined the cellular signature of the VT CI in vivo as a region of exceptional enrichment of MFB, which interconnected the few remaining clusters of CM in damaged regions of the myocardium. This finding provided a plausible explanation of electrical inhomogeneity and the basis for pro-VT inducibility and slow conduction.

ACKNOWLEDGEMENT The authors thank Biosense-Webster for technical support throughout the project.

ADDRESS FOR CORRESPONDENCE: Dr. Christopher H. George, Swansea University Medical School, Institute of Life Sciences, Singleton Park, Swansea, Wales SA2 8PP, United Kingdom. E-mail: chg.swansea@gmail.com.

PERSPECTIVES

COMPETENCY IN MEDICAL KNOWLEDGE: Post-infarction re-entrant VT infers a high risk of sudden death. Electroanatomical- and magnetic resonance imaging-based mapping techniques have defined the initiation site of the VT circuit as heterogeneous areas of myocardium interwoven with scar, which is termed the CI. The CI is a target for catheter-based VT ablation. However, despite the increasing numbers of procedures being performed, the long-term success rate of catheter ablation, when measured in terms of freedom from any recurrent VT, remains suboptimal.

TRANSLATIONAL OUTLOOK 1: Analysis of EP-mapped areas of scar defined the cellular composition of the CI as a morphologic zone characterized by small clusters of CM interspersed by exceptionally high numbers of stromal cells (FB, MFB). Our data suggested that the massive accumulation of MFB represent the cellular substrate for VT inducibility.

TRANSLATIONAL OUTLOOK 2: This research advanced our understanding of the cellular and molecular interactions at the VT CI, with the potential to identify unique cellular markers that define the CI. This will enable the development of imaging-based markers to aid catheter ablation and help improve the long-term procedural success rates. This research underpins the potential future development of cell-targeted pharmacologies for VT ablation.

REFERENCES

1. de Bakker JM, van Capelle FJ, Janse MJ, et al. Slow conduction in the infarcted human heart. 'Zigzag' course of activation. Circulation 1993;88:915–26.

2. Stevenson WG, Soejima K. Catheter ablation for ventricular tachycardia. Circulation 2007;115:2750–60.

3. Josephson ME, Horowitz LN, Farshidi A. Continuous local electrical activity. A mechanism of recurrent ventricular tachycardia. Circulation 1978;57:659–65.

4. Stevenson WG, Weiss JN, Wiener I, Nademanee K. Slow conduction in the infarct scar: relevance to the occurrence, detection, and ablation of ventricular reentry circuits resulting from myocardial infarction. Am Heart J 1989;117:452–67.

5. Stevenson WG, Khan H, Sager P, et al. Identification of reentry circuit sites during catheter mapping and radiofrequency ablation of ventricular tachycardia late after myocardial infarction. Circulation 1993;88:1647–70.

6. Brunckhorst CB, Stevenson WG, Soejima K, et al. Relationship of slow conduction detected by pace-mapping to ventricular tachycardia re-entry circuit sites after infarction. J Am Coll Cardiol 2003;41:802–9.

7. Ashikaga H, Sasano T, Dong J, et al. Magnetic resonance-based anatomical analysis of scar-related ventricular tachycardia: implications for catheter ablation. Circ Res 2007;101:939–47.

8. Schmidt A, Azevedo CF, Cheng A, et al. Infarct tissue heterogeneity by magnetic resonance imaging identifies enhanced cardiac arrhythmia susceptibility in patients with left ventricular dysfunction. Circulation 2007;115:2006–14.

9. Estner HL, Zviman MM, Herzka D, et al. The critical isthmus sites of ischemic ventricular tachycardia are in zones of tissue heterogeneity,

visualized by magnetic resonance imaging. Heart Rhythm 2011;8:1942–9.

10. Rog-Zielinska EA, Norris RA, Kohl P, Markwald R. The living scar–cardiac fibroblasts and the injured heart. Trends Mol Med 2016;22:99–114.

11. Baba S, Dun W, Cabo C, Boyden PA. Remodeling in cells from different regions of the reentrant circuit during ventricular tachycardia. Circulation 2005;112:2386–96.

12. Hermans KCM, Daskalopoulos EP, Blankesteijn WM. The Janus face of myofibroblasts in the remodeling heart. J Mol Cell Cardiol 2016;91:35–41.

13. Moore-Morris T, Cattaneo P, Puceat M, Evans SM. Origins of cardiac fibroblasts. J Mol Cell Cardiol 2016;91:1–5.

14. Davis J, Molkentin JD. Myofibroblasts: trust your heart and let fate decide. J Mol Cell Cardiol 2014;70:9–18.

15. Turner NA, Porter KE. Function and fate of myofibroblasts after myocardial infarction. Fibro Tissue Rep 2013;6:5.

16. Travers JG, Kamal FA, Robbins J, Yutzey KE, Blaxall BC. Cardiac fibrosis: the fibroblast awakens. Circ Res 2016;118:1021–40.

17. Kaur K, Zarzoso M, Ponce-Balbuena D, et al. TGF-β1, released by myofibroblasts, differentially regulates transcription and function of sodium and potassium channels in adult rat ventricular myocytes. PLoS One 2013;8:e55391.

18. Rosker C, Salvarani N, Schmutz S, Grand T, Rohr S. Abolishing myofibroblast arrhythmogeneicity by pharmacological ablation of α-smooth muscle actin containing stress fibers. Circ Res 2011;109:1120–31.

19. Camelliti P, Borg TK, Kohl P. Structural and functional characterisation of cardiac fibroblasts. Cardiovasc Res 2005;65:40–51.

20. Kohl P, Gourdie RG. Fibroblast-myocyte electrotonic coupling: does it occur in native cardiac tissue? J Mol Cell Cardiol 2014;70:37–46.

21. Callans DJ, Ren J-F, Michele J, Marchlinski FE, Dillon SM. Electroanatomic left ventricular mapping in the porcine model of healed anterior myocardial infarction: correlation with intracardiac echocardiography and pathological analysis. Circulation 1999;100:1744–50.

22. Reddy VY, Wrobleski D, Houghtaling C, Josephson ME, Ruskin JN. Combined epicardial and endocardial electroanatomic mapping in a porcine model of healed myocardial infarction. Circulation 2003;107:3236–42.

23. Sasano T, Keleman K, Greener ID, Donahue JK. Ventricular tachycardia from the healed myocardial infarction scar: validation of an animal model and utility of gene therapy. Heart Rhythm 2009;6:S91–7.

24. Anter E, Tschabrunn CM, Buxton AE, Josephson ME. High-resolution mapping of post-infarction reentrant ventricular tachycardia. Circulation 2016;134:314–27.

25. Kilkenny C, Browne WJ, Cuthill IC, Emerson M, Altman DG. Improving bioscience research reporting: the ARRIVE guidelines for reporting animal research. PLoS Biol 2010;8:e1000412.

26. Soejima K, Stevenson WG, Maisel WH, Sapp JL, Epstein LM. Electrically unexcitable scar mapping based on pacing threshold for identification of the reentry circuit isthmus: feasibility for guiding ventricular tachycardia ablation. Circulation 2002;106:1678–83.

27. Sasano T, McDonald AD, Kikuchi K, Donahue JK. Molecular ablation of ventricular tachycardia after myocardial infarction. Nat Med 2006;12:1256–8.

28. Stevenson WG, Sager PT, Natterson PD, Saxon LA, Middlekauff HR, Wiener I. Relation of pace mapping QRS configuration and conduction delay to ventricular tachycardia reentry circuits in human infarct scars. J Am Coll Cardiol 1995;26:481–8.

29. Jäis P, Maury P, Khairy P, et al. Elimination of local abnormal ventricular activities: a new end point for substrate modification in patients with scar-related ventricular tachycardia. Circulation 2012;125:2184–96.

30. Mollmann H, Nef HM, Kostin S, et al. Bone marrow-derived cells contribute to infarct remodelling. Cardiovasc Res 2006;71:661–71.

31. Takemura G, Ohno M, Hayakawa Y, et al. Role of apoptosis in the disappearance of infiltrated and proliferated interstitial cells after myocardial infarction. Circ Res 1998;82:1130–8.

32. Gepstein L, Hayam G, Ben-Haim SA. A novel method for nonfluoroscopic catheter-based electroanatomical mapping of the heart. In vitro and in vivo accuracy results. Circulation 1997;95:1611–22.

33. Curtis MJ, Hancox JC, Farkas A, et al. The Lambeth Conventions (II): guidelines for the study of animal and human ventricular and supraventricular arrhythmias. Pharm Ther 2013;139:213–48.

34. Camelliti P, Green CR, LeGrice I, Kohl P. Fibroblast network in rabbit sinoatrial node: structural and functional identification of homogeneous and heterogeneous cell coupling. Circ Res 2004;94:828–35.

KEY WORDS border zone, critical isthmus, myocardial infarction, myofibroblasts, pig, VT

APPENDIX For an expanded Methods section as well as a supplemental table and figures, please see the online version of this paper.

Go to http://www.acc.org/jacc-journals-cme to take the CME/MOC quiz for this article.